JPL D-110523

Surface Biology and Geology (SBG) Observing Terrestrial Thermal Emission Radiometer (OTTER)

Level 1 Geometric Calibration Algorithm Theoretical Basis Document (ATBD)

Version 0.5
September 01, 2023

Michael M. Smyth
Level 1 Algorithms Team
Jet Propulsion Laboratory
California Institute of Technology

National Aeronautics and
Space Administration

Jet Propulsion Laboratory
4800 Oak Grove Drive
Pasadena, California 91109-8099
California Institute of Technology

This research was carried out at the Jet Propulsion Laboratory, California Institute of Technology, under a contract with the National Aeronautics and Space Administration.

Change History Log

Revision	Effective Date	Prepared by	Description of Changes
Draft	09/01/2023	M. Smyth	SBG-TIR L1 Geolocation ATBD first draft.

Contacts

Readers seeking additional information about this study may contact the following:

Mike M. Smyth
MS 168-421
Jet Propulsion Laboratory
California Institute of Technology
4800 Oak Grove Dr.
Pasadena, CA 91109
Email: *mike.m.smyth@jpl.nasa.gov*
Office: (818) 354-9812

Thomas L. Logan
MS 168-414
Jet Propulsion Laboratory
California Institute of Technology
4800 Oak Grove Dr.
Pasadena, CA 91109
Email: *thomas.l.logan@jpl.nasa.gov*
Office: (818) 354-4032

This Page Intentional Left Blank.

Abstract / Background

In 2021, the NASA Earth System Observatory (ESO) identified the study of Surface Biology and Geology (SBG) as one of five science focus areas based on recommendations from the 2018 Decadal Survey. The concept's implementation has since evolved into two separate spacecraft platform systems: A VSWIR (Visible and Short Wave Infrared imaging spectrometer) for hyperspectral analysis, and dual VNIR (Visible and Near Infrared) and TIR (Thermal Infrared) instruments for focused thermal mapping science [1]. This document specifically addresses geolocation of the SBG-TIR instrument aboard the second platform.

The SBG-TIR instrument, also known as "OTTER" (Orbiting Terrestrial Thermal Emission Radiometer), was designed and built by the Jet Propulsion Laboratory (JPL). It is mounted to a free-flyer satellite platform built and managed by the Italian Space Agency (ASI), who also manages the separate (co-boresighted) VNIR camera. The TIR instrument's focus is exploration of the Earth's surface temperature and emissivity, evapotranspiration, vegetative water stress, substrate composition, volcanic plumes, and other high-temperature features and their change over time. The instrument uses a continuously rotating scan mirror in a push-whisk configuration to direct light from the telescope through eight narrowband interference filters to the Focal Plane Array (FPA). The eight bands include two mid-infrared wavelengths (3-5μm) and six thermal wavelengths (8-12μm). (The VNIR camera provides three additional spectral bands managed by ASI.) The platform will have an operational altitude of ~693km providing an approximate ground sample distance (GSD) of 60m at nadir, and an image granule size of approximately 910x1060km with 3-day repeat visit time.

This algorithm theoretical basis document (ATBD) describes the Level 1 geolocation of the SGB-TIR OTTER imagery. The geolocation strategy depends on the characteristics of the acquired scenes. For standard daytime time, the corrected ephemeris and attitude data from the higher resolution ASI VNIR instrument are used. When VNIR data are not available (e.g., nighttime data) we will perform image matching against an existing ortho-base and use this to correct errors in the ephemeris and attitude. A pointing model is then used with the corrected ephemeris and attitude to calculate surface latitude and longitude for each image pixel, along with related ancillary metadata (view angles, solar angles). Depending on the geolocation strategy used, the expected geolocation accuracy is TBD (VNIR), will be better than 57 m (image matching), or 120 m (uncorrected ephemeris and attitude).

Table of Contents

Figures

Tables

1 Introduction

The OTTER (Orbiting Terrestrial Thermal Emission Radiometer) is part of the NASA SBG (Surface Biology and Geology) mission that deploys an advanced imaging spectrometer on a “free-flyer” space platform managed by the Italian Space Agency (ASI) to monitor Earth environment temperatures using Thermal Infrared (TIR) wavelengths [1]. The planned science focus includes surface radiance, temperature, emissivity, evapotranspiration, volcanic plumes, water use efficiency, and related temperature manifestations. To measure radiance, the instrument uses a continuously rotating scan mirror in a push-whisk configuration to direct light from the telescope through eight narrowband interference filters to the Focal Plane Array (FPA). The focal plane consists of 8x16x256 arrays of Mercury Cadmium Telluride (MCT) detectors of CMOS (complementary metal oxide semiconductor) manufacture. The OTTER FPA design is an update of the “Prototype HyspIRI-TIR (PHyTIR)” instrument originally developed at JPL by Johnson, et al [2], and flown by the NASA ECOSTRESS Mission [3] aboard the ISS (International Space Station). A summary of OTTER spectral imaging parameters is provided as Table 1.

Band Number	**Center Wavelength (microns)**	**Bandwidth (microns)**	**Pixel GSD (Nadir):** 60 x 60m
4	3.98	0.3 TBD but probably narrower	
5	4.81	0.15	**Earth Coverage Image:**
6	8.32	0.3	910 x 1060km
7	8.63	0.3	**Dynamic Range:**
8	9.07	0.3	14bit Integer
9	10.30	0.3	
10	11.35	0.5	
11	12.05	0.5	

Table 1: The OTTER Spectral Parameters. Note that Band Numbers 1 to 3 are reserved for use by the three VNIR bands (calibrated separately by ASI).

Level-1B Geolocation is the process of generating geotagging information for the SBG-TIR imagery. In addition, related auxiliary information are generated (view angles, solar angles). The DN imagery from L1A processing is converted to physical radiance units, and the data resampled so the 8 bands are coregistered. Finally, orthorectified data is generated as gridded (0.0006 degree latitude/longitude) and tiled (60m UTM, Sentinel tile) products. The tiled product will also include the separate instrument VNIR data, averaged to the same 60 m UTM tile.

Level-1B is part of the overall Level 1 data flow, as shown in Figure 1-1.

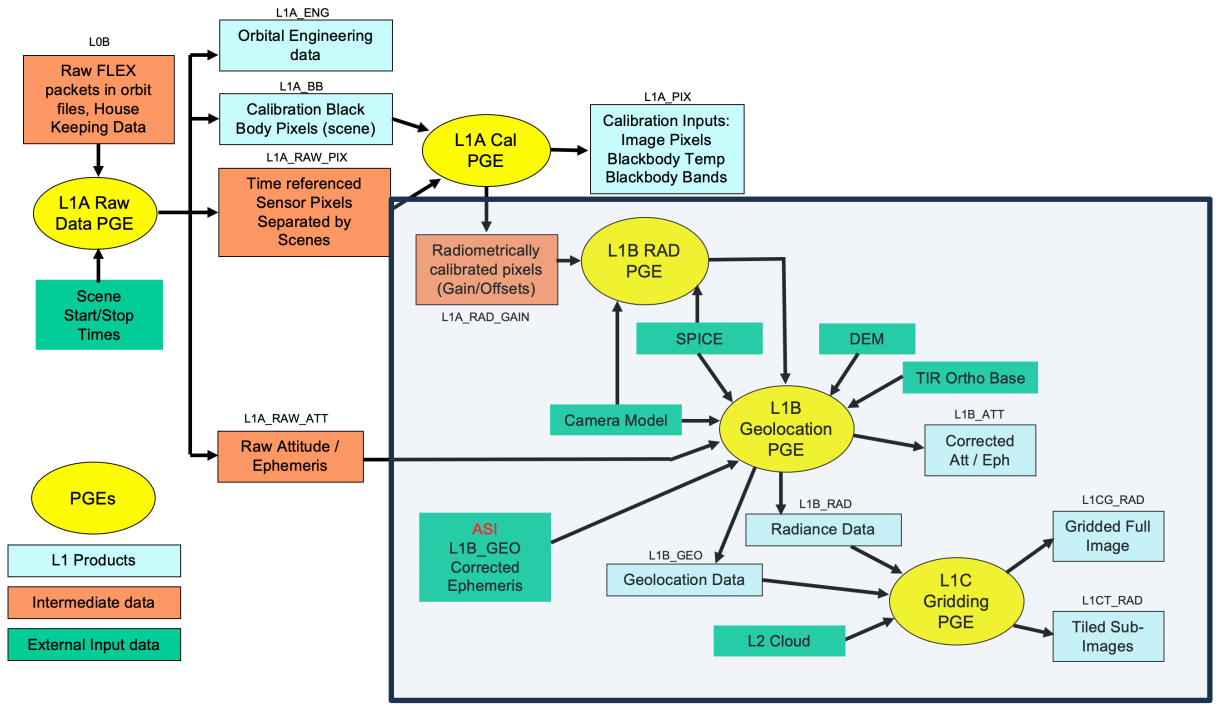

Figure 1-1: SBG-TIR Level 1 PGE Product Data Flow

2 Input datasets

The input datasets to the L1B Geo processing are shown in the following table:

Ephemeris data	Gives position of spacecraft
Attitude data	Gives pointing of spacecraft
Corrected ephemeris/attitude from ASI VNIR instrument	Corrected pointing, only available for standard daylight scenes
Camera model	Describe orientation of sensor with spacecraft and pointing information for each pixel (interior and exterior orientation)
DEM	Provide height range used in creating RSM
Orthobase	Provides ground truth for image matching when ASI VNIR corrected

		ephemeris/attitude not available.
SPICE Kernels	Leapseconds	Provide information about leap seconds
	Utcpole	Provide orientation of earth with inertial base frame (include UT1-UTC, precision, polar motion)
	Solar ephemeris	Location of sun relative to earth

Table 2: Input data sets

3 Geolocation Based on Image Matching

3.1 SBG TIR Instrument Geometry and Optical Distortion

The SBG-TIR instrument operates as a push-whisk scanner, collecting 256 pixels in the cross-whisk direction for each spectral channel, which enables a wide swath and high spatial resolution. As the platform moves forward, the scan mirror sweeps the focal plane ground projection in the cross-track direction. The different spectral bands are swept across a given point on the ground sequentially. From the 665 km (TBD) altitude, the resulting swath is 935 km (TBD) wide. A conceptual layout for the instrument is shown in Figure 3-1. The scan mirror rotates at a constant angular speed. It sweeps the focal plane image 68.8° (TBD) across nadir.

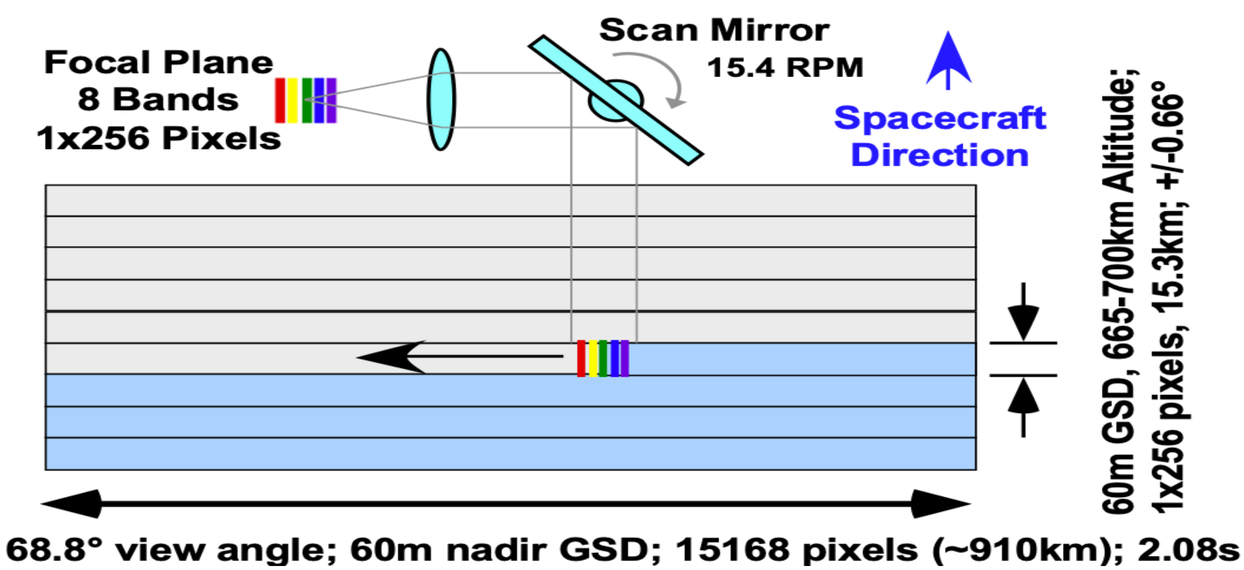

Figure 3-1: SBG-TIR scanning scheme.

Figure 3-2 provides a more detailed view of the focal plane array, with corresponding axis along the scanning and cross-scanning directions. Compared to the ground velocity, the high scanning velocity during the sensor dwell time of TBD μs produces a smearing of the pixels along the scanning direction, resulting in an effective nadir resolution of 60 m TBD along the sensor Y direction (scan direction).

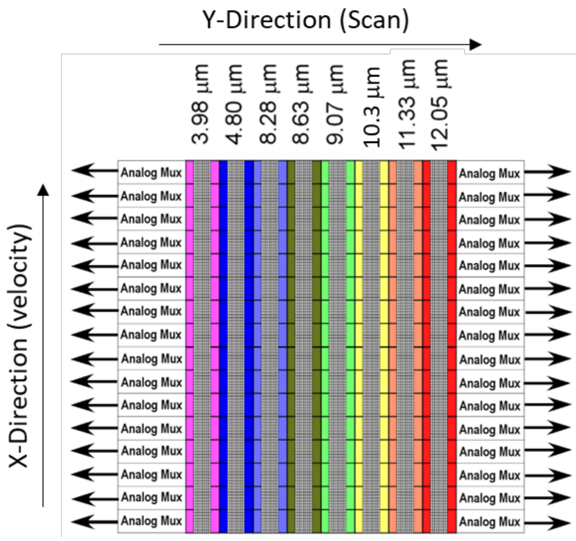

Figure 3-2: Focal plane axis convention. Y is the scanning direction and X the cross-scan (velocity) direction. OTTER

There is very little optical distortion (TBD, reference camera model from Bill Johnson), however the bands are separated on the ground. The data is resampled to produce coregistered data, as described in Section 3.5.

3.2 SBG Pointing Model

Geolocation is derived by propagating the instrument pointing model from the payload through the different elements, until it is intersected with the ground topography. These next sections formulate this back-propagation of light from the focal plane back to the ground location it originated from.

The rigorous model provides a mapping from image pixel (u, v) and time t to a look vector $\vec{L}_{ECEF}$ in ECEF coordinates. $\vec{L}_{ECEF}$ is a unit vector that points in the direction the image pixel (u, v) looks. Given $\vec{L}_{ECEF}$ along with the position $\vec{P}_{ECEF}$ of the spacecraft we can then calculate the ground location viewed at a given height.

The mapping from (u, v, t) to $\vec{L}_{ECEF}$ and $\vec{P}_{ECEF}$ occurs in a number of steps:

$$\vec{L}_{ECEF} = T^t_{OCS\ to\ ECEF} \circ T_{SC\ to\ OCS} \circ T_{SM\ to\ SC} \circ T_{SM\ to\ SC}(u)(\vec{L}_{ICS}(0, v, b))$$

$$\vec{P}_{ECEF} = T^t_{ECI\ to\ ECEF}(\vec{P}_{ECI}(t))$$

In the next few sections, we will describe each of the transformations, and how we then use the look and position vectors to provide geolocation on an ellipsoid.

3.2.1 Instrument Interior Orientation (Image coordinate to Instrument Reference Frame

3.2.1.1 Interior Orientation

The camera model data is used to generate a look vector $\vec{L}_{ICS}$ for a given image pixel (u, v) for band b. Note that this is the CCD where each band is 1 x 256 (after averaging) so $u = 0$.

The SBG Optics Detector Coordinate Frame is show in Figure 3-3

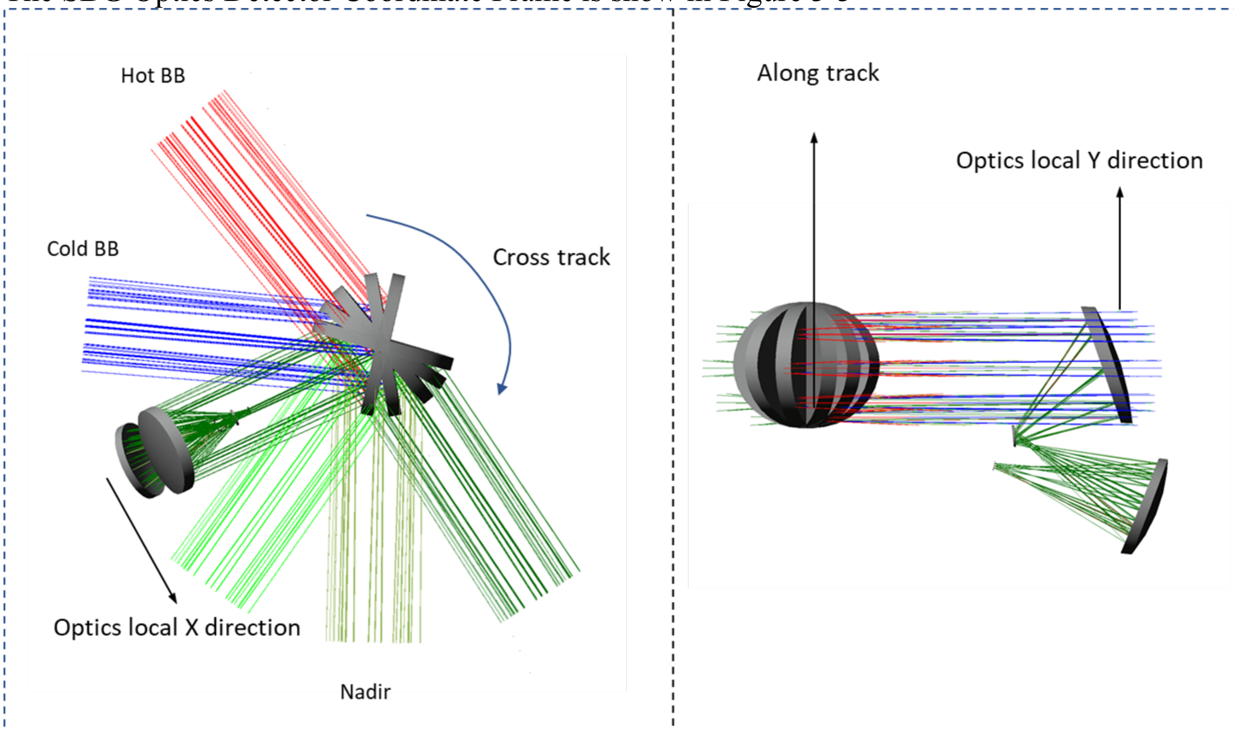

Figure 3-3: Optics coordinate system – OTTER

We start in the detector coordinate system (DCS) which lies in the plane of the focal plane with x-axis in the cross track column or u direction, y-axis in the along track row or v, and z-axis perpendicular to the focal plane. For a strictly linear camera model we can model this as a pinhole camera, giving us:

$$\vec{L}_{DCS}^{Pinhole}(u, v, b) = \begin{bmatrix} (u - u_{p,b})p_u \\ (v - v_{p,b})p_v \\ -f \end{bmatrix}$$

Here the principal point $(u_{p,b}.\, v_{p,b})$, pitch (p_u, p_v) and focal length f come from the camera model. This is for the CCD, so u is 0.

We modify this simple pinhole model to include camera nonlinearities (TBD, description of using field angle map – very similar to ECOSTRESS).

By convention, we scale this to a unit vector:

$$\vec{L}_{DCS}(u,v,b) = \frac{\vec{L}_{DCS}^{unscaled}(u,v,b)}{\left\|\vec{L}_{DCS}^{unscaled}(u,v,b)\right\|}$$

We then rotate this to the instrument coordinate system (ICS), again using information from the camera model, $T_{DCS\ to\ ICS}$:

$$\vec{L}_{ICS}\,(u,v,b) = T_{DCS\ to\ ICS}(\vec{L}_{DCS}(u,v,b))$$

3.2.1.2 Scan Mirror

For each pixel v, with v between 1 and 256, and given a mirror rotation angle $s(u)$ for sample u around the X-axis, we define the instrument pointing model u as follows:

$$\vec{L}_{SM}(u,v,b) = T_{SM\ to\ SC}(u)(\vec{L}_{ICS}\,(0,v,b))$$

$$T_{SM\ to\ SC}(u) = \begin{bmatrix} 1 & 0 & 0 \\ 0 & \cos s(u) & -\sin s(u) \\ 0 & \sin s(u) & \cos s(u) \end{bmatrix}$$

3.2.2 Scan Mirror to Spacecraft

We rotate the scan mirror coordinate system (SM) using the information from the camera model $T_{SM\ to\ SC}$.

$$\vec{L}_{SC}\,(u,v,b) = T_{SM\ to\ SC}(\vec{L}_{SM}(u,v,b))$$

3.2.3 Spacecraft to Orbital

This is a place holder; we need to determine the way this will be described for our spacecraft. The ISS was Euler angles, another very common method is to directly supply a quaternion describing the orientation with the ECI coordinate system.

Attitude of the spacecraft is given as Euler angles between the spacecraft orbital reference system (also called LVLH for “Local Vertical Local Horizontal”) and is described in Figure 3.2-3.

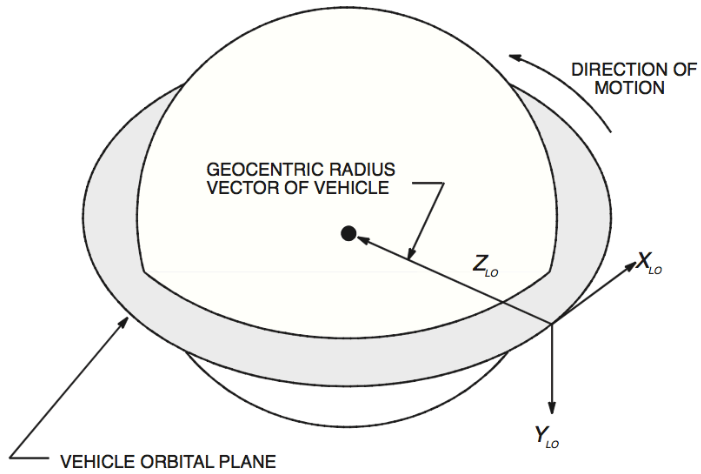

Figure 3.2-3: Orbital reference system definition

Attitude rotation matrices for roll, pitch, and yaw angles are given by:

$$R_{pitch} = \begin{bmatrix} \cos(p) & 0 & \sin(p) \\ 0 & 1 & 0 \\ -\sin(p) & 0 & \cos(p) \end{bmatrix}, R_{roll} = \begin{bmatrix} 1 & 0 & 0 \\ 0 & \cos(r) & -\sin(r) \\ 0 & \sin(r) & \cos(r) \end{bmatrix}, R_{yaw} = \begin{bmatrix} \cos(y) & -\sin(y) & 0 \\ \sin(y) & \cos(y) & 0 \\ 0 & 0 & 1 \end{bmatrix}$$

3.2.4 Orbital to ECI reference frame

This is a place holder; we need to determine the way this will be described for our spacecraft. The ISS was Euler angles, another very common method is to directly supply a quaternion describing the orientation with the ECI coordinate system.

From Figure 3.2.3, we define the orbital reference frame (LVLH) axis as:

$$\begin{cases} \vec{Z}_{LVLH}(t) = -\dfrac{\vec{P}(t)}{\left\|\vec{P}(t)\right\|} \\ \vec{Y}_{LVLH}(t) = \dfrac{\vec{Z}(t)\times\vec{V}(t)}{\left\|\vec{Z}(t)\times\vec{V}(t)\right\|} \\ \vec{X}_{LVLH}(t) = \vec{Y}(t)\times\vec{Z}(t) \end{cases} \tag{1}$$

Where $P(t)$ is the ISS position at time t expressed in Earth-centered inertial (ECI) and $V(t)$ corresponds to the ISS velocity vector at time t, expressed in ECI. Then, we can express the change of reference frame from the Orbital to the ECI reference frame with the matrix:

$$M_{Orb2CTRS} = \begin{bmatrix} X^x_{LVLH} & Y^x_{LVLH} & Z^x_{LVLH} & 0 \\ X^y_{LVLH} & Y^y_{LVLH} & Z^y_{LVLH} & 0 \\ X^z_{LVLH} & Y^z_{LVLH} & Z^z_{LVLH} & 0 \\ 0 & 0 & 0 & 1 \end{bmatrix} \tag{2}$$

3.2.5 ECI to ECF

Spacecraft position is given in Earth-centered inertial (ECI) coordinates. This is the same as the J2000 celestial reference frame. It's North pole or Z axis is along the predicted rotation vector of the Earth at midnight, Jan 1, 2000 AD (JD 2451545.0); its X axis is toward the vernal equinox on that date, and it's Y axis comprises a right handed orthonormal triad with the X and Z axes, in the order X,Y,Z. This frame is nearly inertial; its origin has a small acceleration (~ 0.5 cm/s2) because the Earth goes around the sun, but its axes remain aligned with an inertially fixed set of directions.

For geolocation, we need to convert to Earth-Centered Earth-Fixed (ECEF), also known as ECR ("Earth-Centered Rotational). This gives position in meters. The point (0,0,0) is at the center of the earth, Z-axis goes through true north (which is not the same as the instantaneous earth rotational axis). X-axis intersects the earth at 0 latitude, 0 longitude, and Y-axis completes the right handed coordinate system.

These conversions are handled by standard toolkit libraries, see [4] and [5]. These account for:

1. Precession of Earth's axis. This is the motion of north rotation pole about the ecliptic pole (long term change, due to torques of sun and moon on earth)
2. Nutation of Earth's axis (same source as precision, but shorter term – conventionally the full precession is separate into long and short term components).
3. Axial rotation based on UT1 (Diurnal Earth rotation, including small corrections in the earth rotation rate, unaccounted for can result in as large as 450 meter error)

4. Polar motion. This is small motion of the earth's crust in relation to its rotation as a solid body. This is an about 10 meter correction.

3.2.6 Additional corrections

In addition, there are several corrections to consider:

1. Aberration of Light
2. Light travel time
3. Atmospheric refraction

Aberration of light is the change in view direction due to the relative motion of the spacecraft with earth. This is exactly the same as the apparent movement of stars due to stellar aberration, just pointed downward. This effect is proportional to v/c and is about 5 arcseconds for Low Earth Orbiting spacecraft (LEO). The result on the ground depends on the viewing geometry, but can be 40 meters or so. For a unit look vector, this correction is:

$$\vec{u}_{corr} = \vec{u}_{rest\ frame} + \frac{\vec{v}}{c}$$

Light travel time accounts for the difference that light leave the surface at one time t_1, but the spacecraft has moved when the light arrives at time t_2. This is a small effect for LEO, on the order of 3 meters or so. Because this is so small, we ignore this effect in our pointing model.

Atmospheric refraction affects the view angle from a spacecraft. This can be important for steep viewing angles, but for moderate viewing angles (e.g., up to 45 degrees zenith) the displacement is on the order of 5 meters (see [4] for a discussion of this). Because this is so small, we ignore this effect in our pointing model.

3.2.7 Geolocation on Ellipsoid

We have the expression combining the look vector for image coordinate (u, v) with the position at time t for a distance λ along the look vector of:

$$\vec{X}(t, u, v, b) = \vec{P}_{ECEF}(t) + \lambda \vec{L}_{ECEF}(t, u, v, b)$$

To determine the geolocation with the Earth ellipsoid with elevation h, we determine λ such that X is at the intersection of this ray with the ellipsoid:

$$\frac{X_x^2 + X_y^2}{A^2} + \frac{X_z^2}{B^2} = 1$$

Using the WGS-84 ellipsoid, we have

$$\begin{cases} A = a + h \\ B = b + h \end{cases} \quad \text{with} \begin{cases} a = 6378137m \\ b = 6356752.3142m \end{cases}$$

The equation can be expanded as a second order polynomial and solved. Two solutions will be obtained, the smallest one being the one we are looking for (the other one is the intersection with the other side of the Earth's ellipsoid).

Note that we can easily determine the inverse, given a point on the surface we can determine (u, v) by using a standard root finder.

3.2.8 Geolocation on Surface

Note that as mentioned in the previous section we can easily determine the inverse, given a point on the surface we can determine (u, v) by using a standard root finder. We can include the height term in the location of the surface, as determined by our DEM.

3.3 Error Budget of Geolocation

3.3.1 Geolocation Stability

The expected relative geolocation accuracy during an SBG-TIR scan is 10 m (TBD) (see [7]). The expected stability from one SBG-TIR scan to the next is 10 m (TBD) (see [7]).

3.3.2 Geolocation Accuracy

The ephemeris and attitude reported by the platform will give a geolocation accuracy of 120 m (see [7]). This accuracy will be improved, as described in Section 3.4.

3.4 Geolocation Corrections

We have different strategies for correcting errors in reported ephemeris/attitude, depending on the type of scene we have, described in the following table.

Strategy	When Used	Expected accuracy	Explanation
Use ASI VNIR corrected ephemeris and attitude	Standard Daylight Product	TBD	We make use of this data because it is acquired at a higher resolution of 30 meter so is likely more accurate than we can determine from SBG-TIR alone.
Image matching with ortho-base	Nighttime data, low-latency product, ASI VNIR otherwise not available	57 m	When ASI data isn't available, we fall back to image matching with our orthobase to correct geolocation errors
Use uncorrected ephemeris/attitude	Orbits that have no GCPs (e.g., all ocean)	120 m	When no correction is available, used satellite reported ephemeris/attitude

Table 3: Geolocation correction strategy

The next few subsections describe these correction methods in greater detail.

3.4.1 Geolocation Corrections for SBG Visible (daytime corrections)

When available, we use corrected ephemeris and attitude generated by the ASI VNIR Level 1 processing.

While the intention is that the ephemeris and attitude generated is for the platform, in practice it is hard to completely separate the VNIR instrument orientation from corrections applied to the ephemeris and attitude. So, we apply a correction:

$$\vec{L}_{TIR}\,(u,v) = T_{VNIR\ to\ TIR}(\vec{L}_{VNIR}(u,v))$$
$$T_{VNIR\ to\ TIR} = R_{pitch}R_{roll}R_{yaw}$$

$$R_{pitch} = \begin{bmatrix} \cos(p) & 0 & \sin(p) \\ 0 & 1 & 0 \\ -\sin(p) & 0 & \cos(p) \end{bmatrix}, R_{roll} = \begin{bmatrix} 1 & 0 & 0 \\ 0 & \cos(r) & -\sin(r) \\ 0 & \sin(r) & \cos(r) \end{bmatrix}, R_{yaw} = \begin{bmatrix} \cos(y) & -\sin(y) & 0 \\ \sin(y) & \cos(y) & 0 \\ 0 & 0 & 1 \end{bmatrix}$$

Early in the mission, we calibrate the yaw, pitch and roll angles needed to account for any difference between the VNIR corrected ephemeris/attitude and the SBG-TIR corrected ephemeris/attitude. These values are nominally 0, and expected to be small. We expect to achieve a geolocation accuracy on the order of TBD (see [7]).

3.4.2 Geolocation Corrections Based on Image Matching (nighttime, low latency product, ASI not available)

Analysis of the geolocation uncertainties in the previous section concluded that the primary source of error could be attributed to lack of knowledge of absolute ephemeris and attitude angles. However, relative attitude information is known with sufficient accuracy that the corresponding geolocation error should account for less than a fraction of the SBG-TIR pixel size. Therefore, at the time-scale of a given scene, accurate absolute geolocation can be achieved by solving for a constant offset correction on the ephemeris and attitude data. In practice, we usually solve for an affine or a quadratic correction rather than just an offset to account for potential other unknown errors, if the number of ground control points allows such correction to be reliable.

The general principle to correct for the absolute geolocation error is to gather ground control points (GCPs) within each scene in order to solve for the missing absolute attitude information. GCPs information are propagated back to the ray-tracing model and a correction model is updated such that error with the GCPs is minimized. In practice, GCPs are gathered automatically using radiance image matching between an ortho-rectified reference and the given rectified SBG-TIR frame with uncorrected ephemeris/attitude geolocation uncertainty. The general scheme borrows from and is illustrated in Figure 3-4:

1. Generate an ortho-rectified SBG-TIR image based on the SBG-TIR camera model initially located with uncorrected pointing and position information.
2. Apply radiance image algorithm between the SBG-TIR rectified radiance image and the accurately geolocated reference Landsat imagery. Image matching is performed using Fourier phase correlation, as described in (see [8] and [9]).
3. Filter out mismatches and produce GCPs.
4. Use GCPs to update SBG-TIR projection model.
5. Potentially iterate steps 1-4.
6. Deliver corrected geolocation information for all image pixels for the SBG-TIR scene.

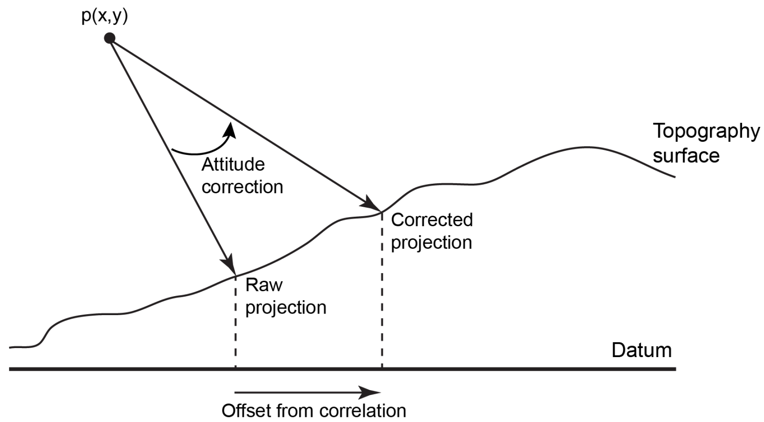

Figure 3-4: General scheme to update EMIT absolute attitude uncertainty.

The geolocation accuracy after correction should match the level of accuracy given by the image matching. Fourier phase correlation methods have demonstrated matching accuracy to be better than 1/10 of the pixel size.

The Landsat reference imaging has excellent absolute geolocation accuracy. SBG-TIR imagery matching is expected to achieve a geolocation accuracy on the order of 57m 1-sigma (see [7]).

3.4.3 Geolocation Correction Interpolation/Extrapolation

It is frequently the case that for a particular scene image matching with the global ortho-base cannot be performed. This might occur because scenes are over water, or the scenes are cloudy, or we just have scenes without a lot of features to match. To accommodate this, we look at all scenes in the orbit. If we successfully match any of the scenes, then corrections from that scene can be applied to all the scenes in the orbit (see Figure 3-5). This works because although the attitude knowledge error can be large, it is slowly varying.

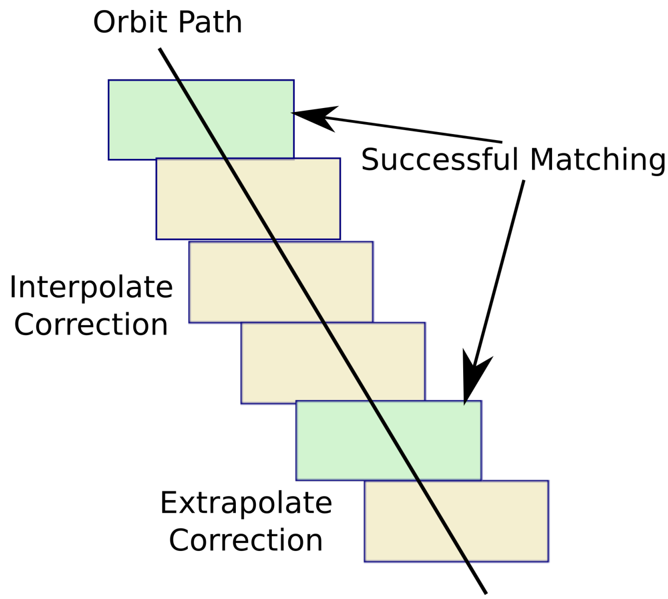

Figure 3-5: Interpolating/Extrapolating Corrections

3.4.4 Uncorrected geolocation (orbits with no GCPs, e.g., all ocean)

In some cases we will not have ASI VNIR corrected ephemeris/attitude available, and will not be able to use image matching for correcting the ephemeris and attitude. This might happen for example for an orbit with a large amount of cloud over land, or for an orbit where only ocean data is collected.

In case we cannot correct the data, we use the uncorrected ephemeris and attitude data. Even with uncorrected data, we expect to achieve geolocation accuracy of 120m (see [7]).

3.5 Band to band co-registration

The 8 bands of the SBG-TIR instrument are offset from each other on the ground. As part of the L1B Calibration, we resample 7 of the bands to co-register with a TBD reference band.

The coregistration is done by first collecting a grid of conjugate points. We determine where image coordinate (u_{ref}, v_{ref}) appears on the ground (using uncorrected ephemeris/attitude), and then determine where that point on the ground is seen in band b, giving (u_b, v_b).

Note that any errors in the uncorrected ephemeris/attitude is close to cancelling when we do this round-trip calculation, the (u_b, v_b) calculated with uncorrected ephemeris/attitude is very close to what we would get with corrected ephemeris/attitude.

We then fit a TBD model to the conjugate points (e.g., a quadratic model). This model is used to resample band b image to the reference band image. We expect to achieve an accuracy of 0.3 pixel coregistration (see [7]).

The band to band registration is applied as part of the L1B RAD PGE, which also uses the coefficients form the L1A Cal PGE to convert the L1A DN values to radiance values (Watt/m2/sr/um) with coregistered bands. See Figure 3-6.

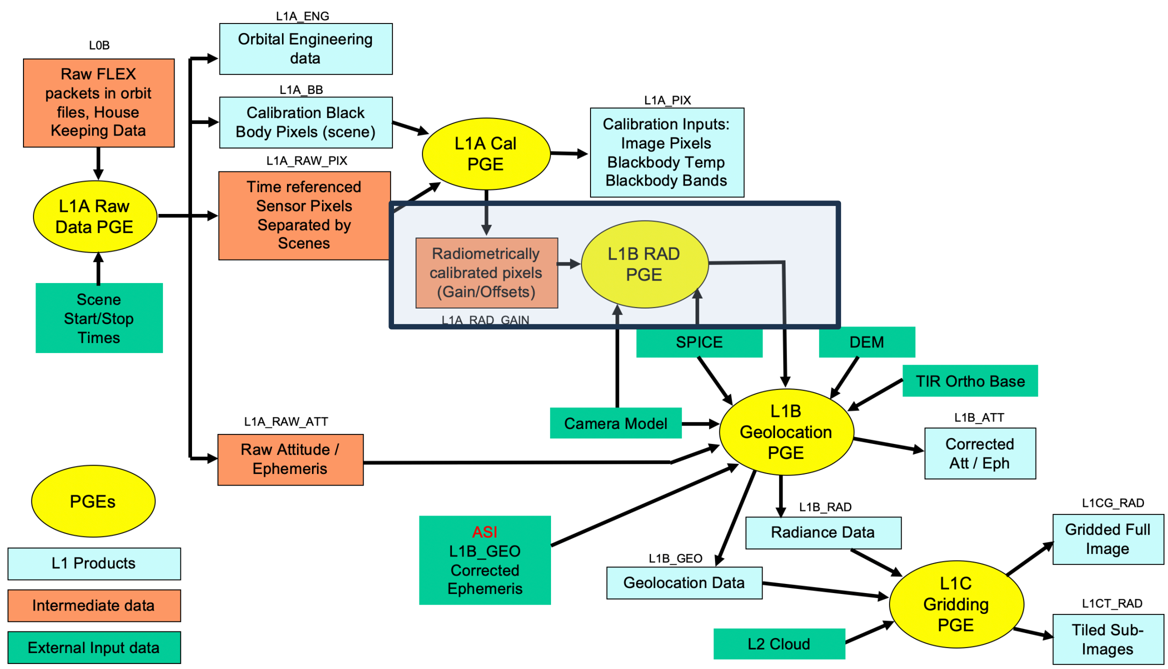

Figure 3-6: SBG-TIR Level 1 PGE Product Data Flow – L1B RAD PGE

3.6 Auxiliary metadata

We calculate view angles and solar angles. This is done by converting the view and sun look vectors to a Local North (LN) coordinate system and then giving the zenith and azimuth angles in that coordinate system.

Local North (LN) coordinate system is a local tangent plane at a view location with X in the east direction, Y in the north direction, and Z in the up direction (also called "ENU"). If ϕ and λ are the geodetic latitude and longitude, then the rotation from ECEF to local north is given by (see [4]):

$$R_{LN\ to\ ECEF} = \begin{bmatrix} \sin\lambda & -\cos\lambda\sin\phi & \cos\lambda\cos\phi \\ \cos\lambda & -\sin\lambda\cos\phi & \sin\lambda\cos\phi \\ 0 & \cos\phi & \sin\phi \end{bmatrix}$$

$$R_{ECEF\ to\ lN} = R^T_{LN\ to\ ECEF}$$

Given a view vector L_{ECEF} we calculate $L_{LN} = R_{ECEF\ to\ LN} L_{ECEF}$ and then have view zenith and azimuth of

$$\theta = \cos^{-1} L_z^{LN}$$

$$\phi = \tan^{-1}\frac{L_x^{LN}}{L_y^{LN}}$$

Likewise, if we have the solar look vector S_{ECEF} we have solar zenith and azimuth of:

$$\theta_0 = \cos^{-1} S_z^{LN}$$

$$\phi_0 = \tan^{-1}\frac{S_x^{LN}}{S_y^{LN}}$$

The auxiliary metadata, along with geotagging (latitude, longitude, height of each image pixel) is done as the L1B Geolocation PGE, see Figure 3-7

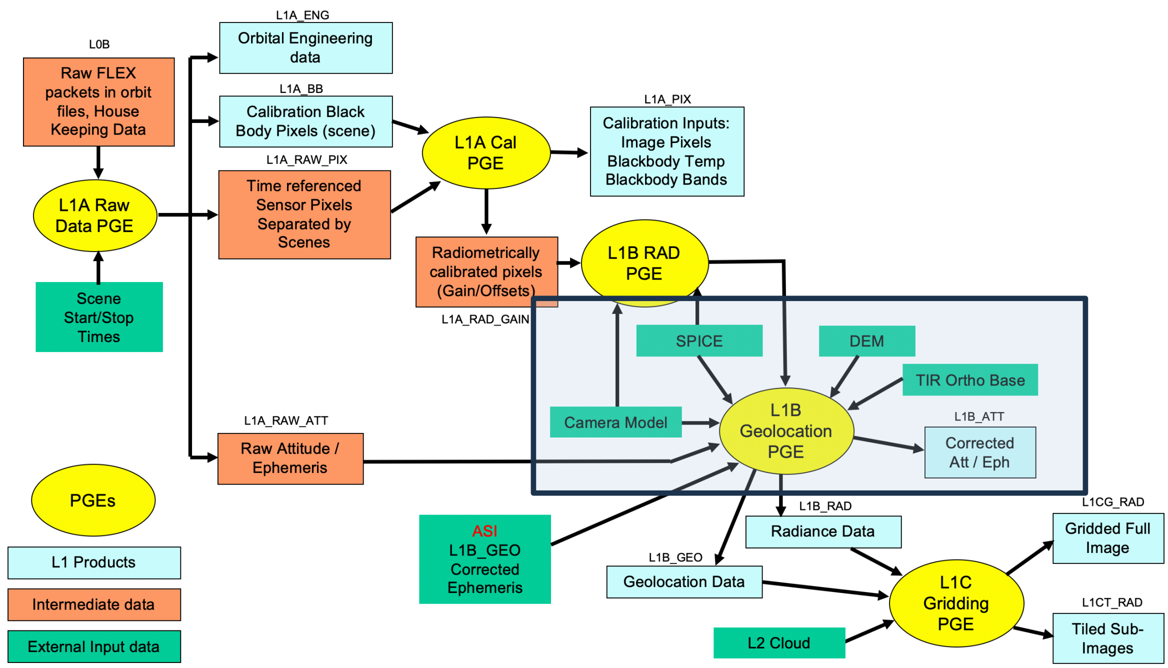

Figure 3-7: SBG-TIR Level 1 PGE Product Data Flow – L1B Geolocation PGE

3.7 Gridded Products

This is a place holder, we are still working out the details of the gridded product. Rather than repeat possibly changing (and potentially out of sync) algorithm, we just refer to the PSD. Once this has been ironed out, we can have a section here describing the details.

Refer to the SBG Gridded L1-L4 Product Specification Document (PSD) for a discussion of L1C gridded products, tiled products, and file formats. Note that in addition to the SBG-TIR data we include the VNIR radiance data resampled to the same 60 m grid as the SBG-TIR data.

See Figure 3-8.

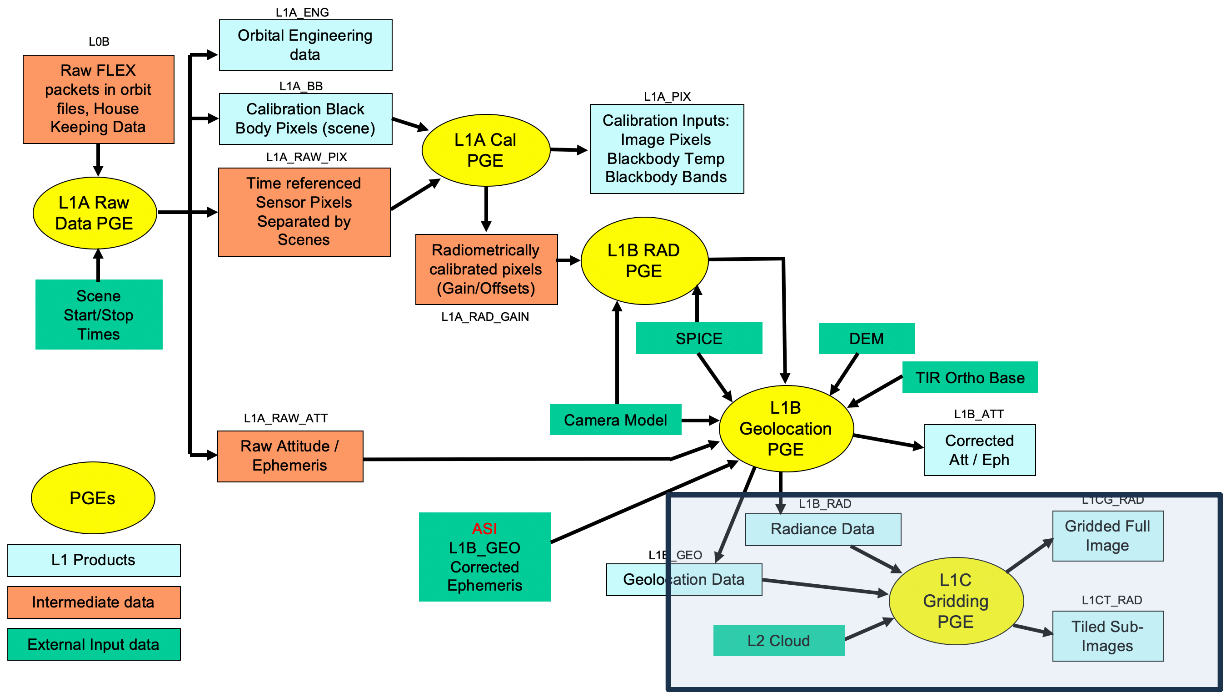

Figure 3-8: SBG-TIR Level 1 PGE Product Data Flow – L1C Gridding PGE

4 Output datasets

The output datasets are shown in the following table:

Output Product	Fields
L1B_RAD (netcdf4)	Radiance data, 8 bands, coregistered
L1B_GEO (netcdf4)	Latitude, Longitude, Height for each image coordinate (u,v)
	View angle zenith, azimuth for each image coordinate (u,v)
	Solar angle zenith, azimuth for each image coordinate (u,v)
L1B_ATT (netcdf4)	Uncorrected ephemeris and attitude
	Corrected ephemeris and attitude
L1C_GRID Rad (COG)	Orthorectified radiance data, 8 bands, 0.0006° grid
L1C_TILE Rad (COG)	Orthorectified radiance data, 8 bands, 60 m UTM grid (Sentinel tiles)

Table 4: Output data sets

5 External Dependencies and Potential Issues

The Level-1B Geolocation depends on corrected ephemeris and attitude from the ASI VNIR instrument. This is used only when available, for standard daytime data. When not available (e.g., nighttime data, low latency product) Level-1B Geolocation processing can be done without the VNIR data.

6 Validation

Placeholder, we need to flesh this out. We'll do a similar validation to what we did with ECOSTRES, with the addition of also comparing with VNIR imagery.

We will validate by manually comparing ortho-rectified SBG-TIR image against our reference ortho-base and the VNIR imagery.

7 References

[1] Basilio, R.R., S.J. Hook, S. Zoffoli, and M.F. Buongiorno, 2022. "Surface Biology and Geology (SBG) Thermal Infrared (TIR) Free-Flyer Concept," 2022 IEEE Aerospace Conference (AERO), Big Sky, MT, USA, 9 pages.

[2] Johnson, W.R., S.J. Hook, M. Foote, B.T. Eng, and B. Jau, 2014. "Characterization and Performance of the Prototype HyspIRI-TIR (PHyTIR) Sensor," Proceedings of SPIE, Vol. 9222, 922208, 12 pages.

[3] NASA/JPL ECOSTRESS (ECOsystem Spaceborne Thermal Radiometer Experiment on Space Station) website. https://ecostress.jpl.nasa.gov/

[4] Noerdlinger, P, 1995. Theoretical Basis of the SPD Toolkit Geolocation Package for ECS Project. 445-TP-002-002

[5] SPICE Toolkit Reference Frames
https://naif.jpl.nasa.gov/pub/naif/toolkit_docs/C/req/frames.html

[6] Jovanovic, V. Algorithm Theoretical Basis and processing software design consideration for GroundMSPI L1B2 process.

[7] Goullioud, R., 2023. "SBG_TIR_Error_Budget_20230828.xlsm," NASA/Jet Propulsion Laboratory internal ECOSTRESS Project Document, California Institute of Technology.

[8] Bryant, Nascier & Zobrist, A. & Logan, T. & Bunch, Walter. (2004). AFIDS, a Precision Automatic Co-Registration Process for Spacecraft Sensors. AGU Fall Meeting Abstracts. -1. 05.

[9] S. Leprince, S. Barbot, F. Ayoub and J. P. Avouac, "Automatic and Precise Ortho-rectification, Coregistration, and Subpixel Correlation of Satellite Images, Application to Ground Deformation Measurements", IEEE Transactions on Geoscience and Remote Sensing, Vol.45, No. 6, June 2007.